EUROPEAN ORGANIZATION FOR NUCLEAR RESEARCH

L3 Note 2564
July 3, 2000

Formation of Light Resonances in $K^0_S K^\pm \pi^\mp$ and $\eta \pi^+ \pi^-$ final states in $\gamma\gamma$ collisions at LEP.

The L3 Collaboration

Abstract

The $e^+e^- \rightarrow e^+e^- K^0_S K^\pm \pi^\mp$ and $e^+e^- \rightarrow e^+e^- \eta \pi^+ \pi^-$ final states are studied with the L3 detector at LEP using data collected at centre of mass energies from 183 to 202 GeV. The mass spectrum of the $K^0_S K^\pm \pi^\mp$ final state shows an enhancement around 1470 MeV, which is identified with the pseudoscalar meson $\eta(1440)$. This state is observed in $\gamma\gamma$ collisions for the first time and the value of its two–photon width is found to be $\Gamma_{\gamma\gamma}(\eta(1440)) \cdot BR(\eta(1440) \rightarrow K\bar{K}\pi) = 212 \pm 50$ (stat.) $\pm$ 15 (sys.) eV. Clear evidence is obtained for the formation of the axial vector mesons $f_1(1420)$ and $f_1(1285)$. In the $\eta \pi^+ \pi^-$ channel only the $f_1(1285)$ is observed and upper limits for the formation of $\eta(1440)$ and $\eta(1295)$ are given.

Submitted to the
XXXth International Conference on High Energy Physics
Osaka, Japan, July 27 – August 2, 2000.

1 Introduction

Resonance formation in two–photon interactions offers a clean environment to study the spectrum of hadronic final states. In this paper we study the reaction $\gamma\gamma \rightarrow \mathrm{K^0_S\,K^\pm\pi^\mp}$ and $\gamma\gamma \rightarrow \eta\,\pi^+\pi^-$ using data collected by the L3 detector at LEP at $\sqrt{s} = 183 - 202$ GeV with a total integrated luminosity of 449 pb^{-1}.

The mass region between 1200 MeV and 1500 MeV is expected to contain several resonances [1]. For the pseudoscalar sector, the E meson ($M = 1425$ MeV, $\Gamma = 80$ MeV), decaying to $\mathrm{K\bar{K}}\pi$, was first observed in 1963 [2] in $\mathrm{p\bar{p}}$ annihilation at rest. Its quantum numbers were determined to be $J^{PC} = 0^{-+}$, the isospin $I = 0$ being favoured over $I = 1$. A 0^{-+} state, decaying into $\mathrm{K\bar{K}}\pi$, named ι , was also observed in radiative J/ψ decay [3]. The E/ι, classified now as $\eta\,(1440)$ by the Particle Data Group (PDG) [1], was interpreted as a prominent glueball candidate due to its strong production in a gluon rich environment. According to the PDG [1] and a recent measurement of OBELIX Collaboration [4] there are two pseudoscalar in this region: one at lower mass, η_L, which decays into $\mathrm{a_0}\pi$ or directly into $\eta\pi\pi$, and one at higher mass, η_H, reported only in $\mathrm{K\bar{K}}\pi$ final states, decaying to $\mathrm{K^*\,\bar{K}}$. The PDG [1] averages for the $\eta\,(1440)$ states are :

$\eta_L \rightarrow \eta\pi\pi$	$M = 1405 \pm 5$ MeV	$\Gamma = 56 \pm 7$ MeV
$\eta_L \rightarrow \mathrm{K\bar{K}}\pi$	$M = 1419 \pm 1$ MeV	$\Gamma = 59 \pm 5$ MeV
$\eta_H \rightarrow \mathrm{K\bar{K}}\pi$	$M = 1473 \pm 4$ MeV	$\Gamma = 79 \pm 13$ MeV

Until now the $\eta\,(1440)$ has not been observed in two–photon collisions; only upper limits on the two–photon width, $\Gamma_{\gamma\gamma}$, of the order of ~ 1 keV exist [5,6].

If we consider also the $\eta(1295)$, there are three $I = 0$ candidates for the first radial excitation of the pseudoscalar SU(3) nonet. If one of these states is a gluonium, its two–photon width is expected to be small with respect to quarkonia. The gluonium interpretation however is not favoured by lattice gauge theories [8] which predict the 0^{-+} state to be above 2 GeV. More exotic interpretations as a gluonium mixed to $\mathrm{q\bar{q}}$ [9] or a bound state of gluinos [10] were also proposed.

Axial vector mesons ($J^{PC} = 1^{++}$) are also present in these channels with masses close to the $\eta\,(1440)$ mass. The production of spin-1 states is forbidden for real photons, according to the Landau-Yang theorem [11], but it is allowed for virtual photons. The $\mathrm{f_1}(1420)$ was observed in the $\mathrm{K\bar{K}}\pi$ decay mode by the TPC–2γ Collaboration [7] in double–tag events and by the CELLO, JADE and Mark II Collaborations in single–tag events [6,12,13] . Also the $\mathrm{f_1}(1285)$ was seen [7,12] in the $\eta\,\pi^+\pi^-$ decay channel.

In this paper we study the formation of resonances decaying in the low mass region of the $\mathrm{K^0_S\,K^\pm\pi^\mp}$ and $\eta\,\pi^+\pi^-$ final states.

2 Monte Carlo

To describe two–photon resonance formation we use two Monte Carlo generators: EGPC [14] and GaGaRes [15]. The EGPC Monte Carlo describes the two–photon process as a production of two virtual photons and a subsequent formation of a resonance. The luminosity function for transverse photons [16] is used. The resonance is generated with a Breit–Wigner function with mass and width as given by the PDG and $\Gamma_{\gamma\gamma} = 1$ keV. The ratio of the measured cross-section to the cross-section given by the Monte Carlo integration gives then the measurement of $\Gamma_{\gamma\gamma}$. The decay of the resonance is generated according to Lorenz invariant phase-space. The generated events are passed through a full detector simulation using the GEANT [17] and the GEISHA [18] programs and are reconstructed following the same procedure used for the data.

We generated events for all the resonances of interest. For the $K^0_S K^\pm \pi^\mp$ channel we generated resonances at different masses: 1410 MeV, 1440 MeV and 1480 MeV and a full width of 50 MeV. For the $\eta \pi^+\pi^-$ channel we generated a resonance at 1285 MeV with full width of 20 MeV and resonances at 1405 MeV and 1440 MeV with 50 MeV width.

The GaGaRes generator uses the exact matrix element for the process of resonance production like $e^+e^- \rightarrow e^+e^-R$, obtained from the hard scattering approach [19]. It makes it possible to determine the dependence of the two–photon cross section on the photon virtualities. We have re–weighted all the EGPC events with the Q^2 dependence thus obtained for the pseudoscalar and axial vector mesons under investigation.

3 The $e^+e^- \rightarrow e^+e^- K^0_S K^\pm \pi^\mp$ channel

3.1 Event Selection

A detailed description of the L3 detector is given in [20, 21]. The two–photon hadronic events are mainly triggered by the central tracker trigger [22, 23] which requires at least two charged particles, each with $p_t > 150$ MeV, back-to-back, within $\pm 60°$, in the transverse plane.

Events are selected by requiring four charged tracks associated to two vertices: two tracks, $K^\pm\pi^\mp$, associated to the primary vertex, and a K^0_S decaying into $\pi^+\pi^-$ at a secondary vertex. A track must have at least 10 hits out of a maximum of 62. The experimental resolutions depend on the transverse momentum p_T and on the length of the track. The selection cuts are therefore function of these two quantities.

1. Two tracks must be separated from the primary vertex by less than three standard deviations both in the transverse plane and along the beam axis. They must be consistent with a $K^\pm\pi^\mp$ hypothesis with the dE/dx measurement, requiring a confidence level $CL(K\pi) > 0.01$. A pion is identified if $\chi^2_{dE/dx}(\pi) < \chi^2_{dE/dx}(K) - 4$ and a kaon if $\chi^2_{dE/dx}(K) < \chi^2_{dE/dx}(\pi) - 4$. If the particles are not identified, both hypothesis are taken, each with a weight of 0.5.

2. Events with photons are rejected. A photon is defined as an isolated shower, in the polar angular range $0.21 < \theta < 2.93$ rad, with more than one crystal in the electromagnetic calorimeter, with energy of at least 100 MeV. The isolation cut requires no corresponding track inside 0.2 rad, full angle around the photon direction.

The K^0_S is identified by requiring :

- A secondary vertex separated from the primary vertex, in the transverse plane, by at least 3 mm.

- The angle α, in the transverse plane, between the flight direction of the K^0_S candidate (taken as the line between the interaction point and the secondary vertex) and the total transverse momentum vector of the two outgoing tracks must be smaller than 0.2 rad.

- The decay probability of the K^0_S candidate must be compatible with the K^0_S lifetime τ $P(d) = 1 - exp(d\,/\beta\gamma c\tau) \leq 0.99$, where d is the distance in space between the primary and the secondary vertex.

- Both tracks are identified as pions from the dE/dx measurement with CL $> 1\%$.
- The effective mass of the two tracks must be inside the mass region (0.46–0.53) GeV.
- $K^0_S K^0_S$ candidates are excluded. The second K^0_S is defined in the mass range (0.48–0.51) GeV.

To improve further the $K^0_S K^\pm \pi^\mp$ selection additional requirements are used. These requirements are different for events with different total transverse momentum $P_T^2 = (\sum \vec{p_T})^2$, where the sum runs over the four observed particles. For the following analysis we use two samples :

1. <u>*low* P_T^2</u> : For $P_T^2 < 0.2$ GeV^2, the event is accepted if at the primary vertex the two–pion hypothesis has a low confidence level CL$(\pi\pi) < 0.001$ from the dE/dx measurement.
2. <u>*high* P_T^2</u> : For $P_T^2 > 0.2$ GeV^2, the event is accepted if at least one of the two conditions is true :
   a) at the primary vertex CL$(\pi\pi) < 0.001$
   b) particles at the primary vertex have the wire number of the last hit greater than 32 and the probability that the two tracks of the secondary vertex come from the primary vertex is smaller than 30%.

For the low P_T^2 selection sample the dE/dx identification works rather well since the particles have low momentum (Fig. 1). For the high P_T^2 selection sample the dE/dx identification is worse, but the $\pi^+\pi^-\pi^+\pi^-$ background is smaller.

3.2 Results

The low P_T^2 selection results in 290 events for which the $K^0_S K^\pm \pi^\mp$ mass spectrum is shown in Fig. 2. There is a clear enhancement near threshold. The low mass region is fitted with a Gaussian and a second order polynomial background. The fit reproduces the data with a confidence level of 75%, while the confidence level becomes smaller than 10^{-4} if the fit is performed with the background function only. The fit gives 66$\pm$11 events in the peak, a mass $M = 1473 \pm 8$ MeV and $\sigma = 46 \pm 7$ MeV. The mass and width are compatible with the values of the η_H pseudoscalar[1)]. In this region, the Monte Carlo gives an experimental mass resolution $\sigma = 20$ MeV and no systematic shift on the mass value is expected.

The distribution of the total transverse momentum P_T^2, for the mass region 1370$-$1560 MeV, is shown in Fig. 3. The Monte Carlo expectations for the $\eta\,(1440)$ resonance are superimposed to the data. The spectrum shows a rapid decrease, well reproduced by the Monte Carlo up to $P_T^2 \simeq 0.02$ GeV^2. The excess of data at higher P_T^2 can be attributed to the background of two–photon inclusive events, when one or more particles go undetected, and to the contribution of the $f_1(1420)$.

In order to separate $\eta\,(1440)$ and $f_1(1420)$ contributions, the data are subdivided in four P_T^2 bins (Fig. 4) of similar statistics in the resonance region. We notice here that $P_T^2 \simeq Q^2$, where Q^2 is the maximum virtuality of the two photons. The Gaussian plus polynomial fit is repeated for each bin, the results are listed in Table 1. In the highest P_T^2 bin, 1 GeV^2 $< P_T^2$ $<$ 7 GeV^2, also the $f_1(1285)$ is present, we fit this bin with two Gaussians over the polynomial background.

[1)] A Gaussian fit to a Breit–Wigner of $\Gamma = 79$ MeV, convoluted with the resolution function $\sigma = 20$ MeV, gives $\sigma = 47$ MeV.

Although the number of events in each bin is rather small, we observe a slight drift of the mass towards lower values by increasing the P_T^2 of the events.

From the number of events evaluated in the peak in each bin, we measure the cross section $\Delta\sigma$ as a function of P_T^2. The acceptance of the detector, the selection and the trigger efficiencies depend on P_T^2, the combined efficiency ϵ is listed in Table 1. The detector acceptance and the selection efficiency are determined by Monte Carlo, as well as the efficiency of the central tracker trigger (ϵ_{trig} varies from 0.97 at low P_T^2 to 0.74 at the highest P_T^2). All the efficiencies are evaluated with the EGPC Monte Carlo, with uniform decay. The inefficiencies of the higher level triggers are evaluated from the data themselves, they vary somewhat from year to year, ranging from 2% to 8%.

The differential cross-section $d\sigma/dP_T^2$ is shown in Fig. 5. Three hypotheses are tested, using the Q^2 dependence, predicted by GaGaRes Monte Carlo. The presence of a pure pseudoscalar $\eta\,(1440)$ is excluded[2)] with $\mathrm{CL} < 10^{-5}$, due to the high number of events observed at high Q^2. A pure axial-vector meson $\mathrm{f}_1(1420)$ is also excluded with $\mathrm{CL} < 10^{-5}$, due to the strong peak at $Q^2 \simeq 0$. The data are well reproduced by a fit which allows both $\eta\,(1440)$ and $\mathrm{f}_1(1420)$ resonances. Normalising the total number of simulated events to the data, we obtain 72 ± 9 events for the spin–0 particle and 43 ± 9 events for the spin–1, with CL=30%.

The two photon width of the $\eta\,(1440)$ is determined using only events with $P_T^2 < 0.02 GeV^2$ (Fig. 4a). This cut selects events produced by quasi–real photons, dominated by the spin–0 state. Using the result of the fit on the P_T^2 dependence, the contribution of the axial vector meson is estimated to be $(2 \pm 0.4)\%$. This contribution is not corrected for, it is added to the systematic uncertainty. The most important systematic errors are obtained by varying the dE/dx cut (5.1%) and the P_T^2 cut (4.7%).

From the cross section measurement, we obtain

$$\Gamma_{\gamma\gamma}(\eta\,(1440)) \cdot BR(\eta\,(1440) \to \mathrm{K^0_S}(\to \pi^+\pi^-)\mathrm{K}^\pm\pi^\mp) = 49 \pm 12\ (\mathrm{stat.}) \pm 3\ (\mathrm{sys.})\ \mathrm{eV}$$

$$\Gamma_{\gamma\gamma}(\eta\,(1440)) \cdot BR(\eta\,(1440) \to \mathrm{K\bar{K}}\pi) = 212 \pm 50\ (\mathrm{stat.}) \pm 15\ (\mathrm{sys.})\ \mathrm{eV}$$

This value is consistent with the upper limit $\Gamma_{\gamma\gamma}(\eta\,(1440)) \cdot BR(\eta\,(1440) \to \mathrm{K\bar{K}}\pi) < 1.2$ keV reported by the CELLO Collaboration [6].

Looking for intermediate decay states $\mathrm{K^*\,\bar{K}}$ and $\mathrm{a}_0\pi$ we analyse the $\mathrm{K}^\pm\pi$ and $\mathrm{K^0_S K}$ spectra for data with $P_T^2 < 0.2\ \mathrm{GeV}^2$ in the $\eta\,(1440)$ region ($1370 < \mathrm{M}(\mathrm{K^0_S\,K^\pm}\pi^\mp) < 1560$ MeV), Fig. 6. The $\mathrm{K}\pi$ and $\mathrm{K^0_S}\pi$ spectra have enhancements in the mass region between 800 and 900 MeV. A Gaussian fit over a linear background, gives:

for $\mathrm{K}^\pm\pi$: (26±9) events, $M = 870 \pm 10$ MeV and $\sigma = 30 \pm 11$ MeV,

for $\mathrm{K^0_S}\pi$: (40±14) events, $M = 872 \pm 8$ MeV and $\sigma = 34 \pm 8$ MeV and

for the $\mathrm{K}\pi$ combination with the mass closest to the $\mathrm{K}^*(892)$:

(59±10) events, $M = 877 \pm 5$ MeV and $\sigma = 30 \pm 5$ MeV,

consistent with the $\mathrm{K}^*(892)$ parameters. The phase space is rather limited and the $\mathrm{K}^*(892)$ mass bands ($792 < M(\mathrm{K}\pi) < 992$ MeV) overlap with the $\mathrm{a}_0(980)$ mass region ($M(\mathrm{K^0_S K}) < 1100$ MeV), Fig. 7. We consider then the $\mathrm{K^0_S\,K^\pm}\pi^\mp$ spectrum under different conditions (Fig. 8). We observe

- a) For events with at least one $\mathrm{K}\pi$–combination in the K^* mass range ($792 < \mathrm{M}(\mathrm{K}\pi) < 992$ MeV), the Gaussian fit gives:

  (56±9) events, $M = 1479 \pm 9$ MeV and $\sigma = 46 \pm 9$ MeV.

[2)] We used the shape compatibility of the Kolmogorov test.

- b) For events with an a_0 candidate, $M(K^0_S K) < 1100$ MeV, the Gaussian fit gives: (34±7) events, $M = 1446 \pm 16$ MeV and $\sigma = 65 \pm 14$ MeV.
- c)For events with a K^* and no a_0, the Gaussian fit gives: (35±12) events, $M = 1492 \pm 7$ MeV and $\sigma = 32 \pm 9$ MeV.
- d)Requiring the a_0 and no K^* few events are left.
- e) For events with no K^* the signal yield is the same as for no K^* and no a_0 case (f).
- f) For events with no K^* and no a_0, the Gaussian fit gives: (11±4) events, $M = 1442 \pm 8$ MeV and $\sigma = 18 \pm 5$ MeV.

In conclusion the $K^*(892)$ is dominant in the decay, its presence pushes the mass of the $\eta\,(1440)$ toward higher values (point a and c). Lower masses are observed if the $a_0(980)$ is required (point b) or if the $K^*(892)$ is absent (point f). However the limited statistics doesn't allow to draw any firm conclusion about the possible presence of the η_L.

4 The $e^+e^- \to e^+e^-\eta\,\pi^+\pi^-$ channel

4.1 Event Selection

In this channel the decay $\eta \to \gamma\gamma$ is considered, therefore the events are selected by requiring two tracks of opposite charge and two photons. Charged particles and photons are defined as in section 2. The pions are identified by the dE/dx measurement with CL > 1%. For photons we additionally require that the most energetic photon must have energy grater than 300 MeV. The effective mass of the two photons must be inside the η mass range, $(0.47 - 0.62)$ GeV, and a kinematical fit, constrained to the η mass, is applied.

After these cuts, 6444 events are selected with $\eta\,\pi^+\pi^-$ masses below 1750 MeV. The $\eta\,\pi^+\pi^-$ spectrum (Fig. 9a) is dominated at threshold by the $\eta'(958)$ resonance. A Gaussian fit gives $M = 957.7 \pm 0.3$ MeV in perfect agreement with the PDG value. The fitted value $\sigma = 7.9 \pm 0.3$ MeV corresponds to the expected mass resolution in this region. For masses of 1280 MeV and 1400 MeV, the expected resolution is $\sigma = 20$ and 24 MeV respectively.

4.2 Results

The $\eta\,\pi^+\pi^-$ mass spectrum for $P_T^2 < 0.02$ GeV^2 is shown in Fig. 9b. No peak is seen in the region 1200−1480 MeV. The detection efficiency is ϵ =2.0%. It includes the trigger efficiency (which varies in the range 60–75% from year to year) and corrections for the inefficiencies of higher level triggers, ranging from 10% to 35% , depending on the year of data taking.

The absence of a signal gives upper limits, with CL>90%, for the $\eta\,(1440)$ and $\eta\,(1295)$:

$\Gamma_{\gamma\gamma}(\eta\,(1440)) \cdot BR(\eta\,(1440) \to \eta(\to \gamma\gamma)\pi^+\pi^-) < 21$ eV

$\Gamma_{\gamma\gamma}(\eta\,(1440)) \cdot BR(\eta\,(1440) \to \eta\pi\pi) < 80$ eV

$\Gamma_{\gamma\gamma}(\eta\,(1295)) \cdot BR(\eta\,(1295) \to \eta(\to \gamma\gamma)\pi^+\pi^-) < 14$ eV

$\Gamma_{\gamma\gamma}(\eta\,(1295)) \cdot BR(\eta\,(1295) \to \eta\pi\pi) < 55$ eV .

These limits are stronger than the ones established by Crystal Ball Collaboration [5]: $\Gamma_{\gamma\gamma}(\eta\,(1440)) \cdot BR(\eta\,(1440) \to \eta\pi\pi) < 300$ eV and $\Gamma_{\gamma\gamma}(\eta\,(1295)) \cdot BR(\eta\,(1295) \to \eta\pi\pi) <$

300 eV. In Fig. 9c the $\eta\,\pi^+\pi^-$ mass spectrum is plotted for $P_T^2 > 0.02$ GeV^2. A significant signal is observed. A Gaussian fit over a polynomial background gives $M = 1280 \pm 4$ MeV, $\sigma = 20 \pm 3$ MeV and 176 ± 29 events. The absence of this peak at $Q^2 \simeq 0$ (see Fig. 9b) identifies it as a spin–1 state, the fitted parameters correspond to the $\mathrm{f}_1(1285)$.

5 Conclusions

The pseudoscalar meson $\eta\,(1440)$ is observed for the first time in untagged $\gamma\gamma$ collisions in the $\mathrm{K^0_S\,K^{\pm}}\pi^{\mp}$ decay channel. The two–photon width times Branching Ratio is measured to be $\Gamma_{\gamma\gamma}(\eta\,(1440)) \cdot BR(\eta\,(1440) \rightarrow \mathrm{K\bar{K}}\pi) = 212 \pm 50$ (stat.) $\pm$ 15 (sys.) eV. The mass $M = 1473 \pm 8$ MeV is compatible with the value of the η_H pseudoscalar. Events compatible with the $\mathrm{K}^*(892)\mathrm{K}$ and $\mathrm{a}_0(980)\pi$ intermediate final states are observed with a strong overlap. No definite conclusion can be drawn on the presence of the η_L pseudoscalar.

Neither $\eta\,(1440)$ nor $\eta\,(1295)$ are observed in the decay channel $\eta\,\pi^+\pi^-$. The upper limits for their two–photon widths are determined.

The high Q^2 events show clear evidence for the formation of the axial vector mesons $\mathrm{f}_1(1420)$ in the decay channel $\mathrm{K^0_S\,K^{\pm}}\pi^{\mp}$ and $\mathrm{f}_1(1285)$ in both $\mathrm{K^0_S\,K^{\pm}}\pi^{\mp}$ and $\eta\,\pi^+\pi^-$ channels.

Acknowledgements

We wish to express our gratitude to the CERN accelerator division for the excellent performance of the LEP machine. We acknowledge the contributions of all the engineers an technicians who have participated in the construction and maintenance of this experiment.

References

[1] Particle Data Group, C. Caso *et al.*, *Eur. Phys. J.* **C 3** (1998) 1.

[2] R. Armenteros *et al.*, Proc. of the Siena Int. Conf. on Elementary Particles (1963) 287.

[3] Crystal Ball Collaboration, D. L. Scharre *et al.*, *Phys. Lett.* **B 97** (1980) 329.

[4] OBELIX Collaboration, C. Cicalo *et al.*, *Phys. Lett.* **B 462** (1999) 453.

[5] Crystal Ball Collaboration, D. Antreasyan *et al.*, *Phys. Rev.* **D 36** (1987) 2633.

[6] CELLO Collaboration, H. J. Behrend *et al.*, *Z. Phys.* **C 42** (1989) 367.

[7] TPC-2γ Collaboration, H. Aihara *et al.*, *Phys. Lett.* **B209** (1988) 107; Phys. Rev. **D 38** (1988) 1.

[8] G. Bali *et al.Phys. Lett.* **B 309** (1993) 378.

[9] F. Close *et al.*, *Phys. Rev.* **D 55** (1997) 5749.

[10] G. R. Farrar *Phys. Rev. Lett.* **76** (1996) 493.

[11] L. D. Landau, *Dokl. Akad. Nauk. USSR* **60** (1948) 207; C. N. Yang, *Phys. Rev.* **77** (1950) 242.

[12] Mark II Collaboration, G. Gidal *et al.*, *Phys. Rev. Lett.* **59** (1987) 2012; *Phys. Rev. Lett.* . **59** (1987) 2016.

[13] JADE Collaboration, P. Hill *et al.*, *Z. Phys.* **C 42** (1989) 355.

[14] F. L. Linde, "Charm Production in Two–Photon Collisions", Ph. D. Thesis, Rijksuniversiteit Leiden, (1988).

[15] R. van Gulik, *Nucl. Phys.* **B 82** (Proc. Suppl.) (2000) 311.

[16] V. M. Budnev *et al.*, *Phys. Rep.* **C 15** (1975) 181.

[17] R. Brun *et al.*, GEANT 3.15 preprint CERN DD/EE/84-1 (Revised 1987).

[18] H. Fesefeldt, RWTH Aachen report PITHA 85/2 (1985).

[19] G. A. Schuler *et al.*, *Nucl. Phys.* **B 523** (1998) 423.

[20] L3 Collaboration., B. Adeva *et al.*, *Nucl. Inst. Meth.* **A 289** (1990) 35; M. Acciarri *et al.*, *Nucl. Inst. Meth.* **A 351** (1994) 300; M. Chemarin *et al.*, *Nucl. Inst. Meth.* **A 349** (1994) 345; A. Adam *et al.*, *Nucl. Inst. Meth.* **A 383** (1996) 342.

[21] I. C. Brock *et al.*, *Nucl. Inst. Meth.* **A 381** (1996) 236.

[22] P. Béné *et al.*, *Nucl. Inst. Meth.* **A 306** (1991) 150.

[23] D. Haas *et al.*, *Nucl. Inst. Meth.* **A 420** (1999) 101.

ΔP_T^2, GeV^2	Events	M, MeV	Width, MeV	CL, %	ϵ, %	$\Delta\sigma$, pb
$0 - 0.02$	37 ± 9	1481 ± 12	48 ± 9	89	1.03 ± 0.04	8.0 ± 1.9
$0.02 - 0.2$	28 ± 7	1473 ± 11	37 ± 8	77	0.85 ± 0.09	7.4 ± 1.9
$0.2 - 1.$	29 ± 9	1435 ± 10	32 ± 10	99	1.74 ± 0.14	3.7 ± 1.2
$1 - 7$	21 ± 6	1452 ± 11	35 ± 10	55	3.49 ± 0.24	1.4 ± 0.4
$1 - 7$	10 ± 4	1290 ± 12	29 ± 10			

Table 1: Results of the Gaussian plus polynomial background fits performed on the mass spectra of Fig. 4. The number of the events in the Gaussian peak, the mass M and the width σ are listed with the error given by the fit. All fits reproduce the data well, as proven by the confidence level CL value. The partial efficiency ϵ and the partial cross-section $\Delta\sigma$ are also given for each P_T^2 interval.

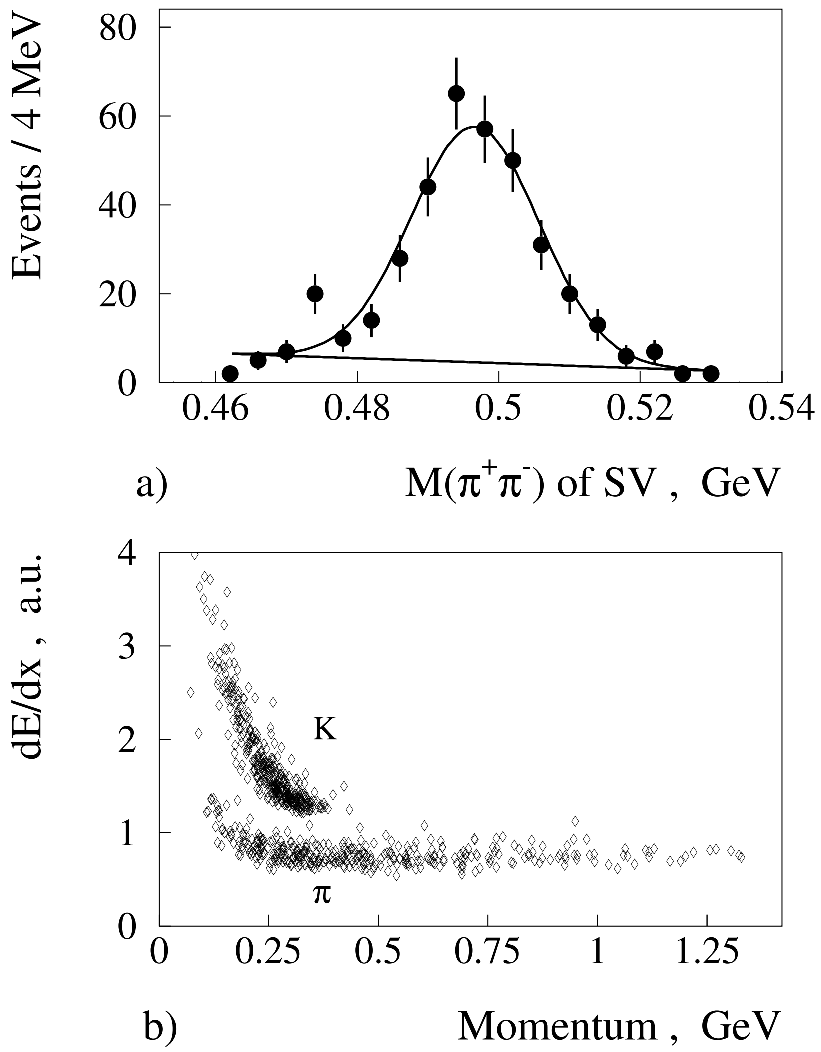

Figure 1: The $K^0_S K^{\pm}\pi^{\mp}$ selection for the low P_T^2 sample. a) The K^0_S mass spectrum. b) dE/dx of kaons and pions at the primary vertex.

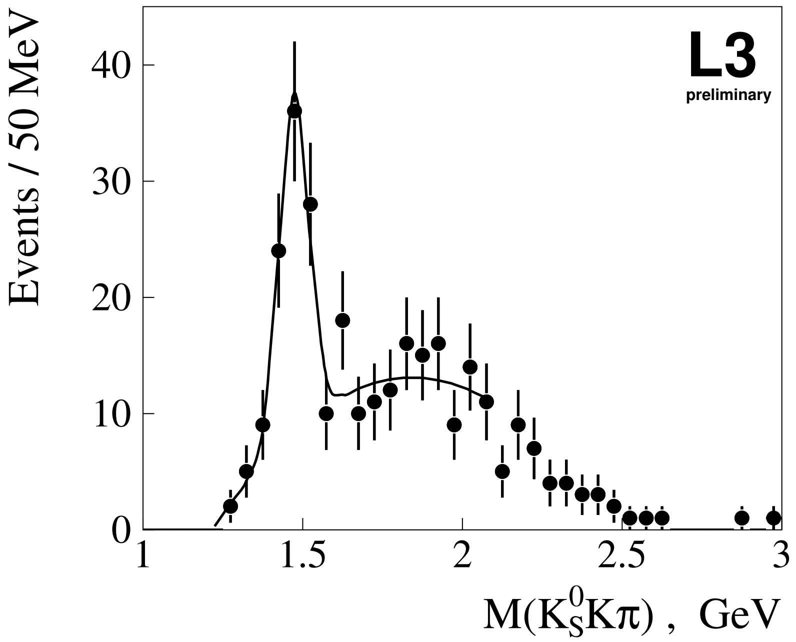

Figure 2: The $K_S^0\,K^{\pm}\pi^{\mp}$ mass spectrum for the low P_T^2 selection sample.

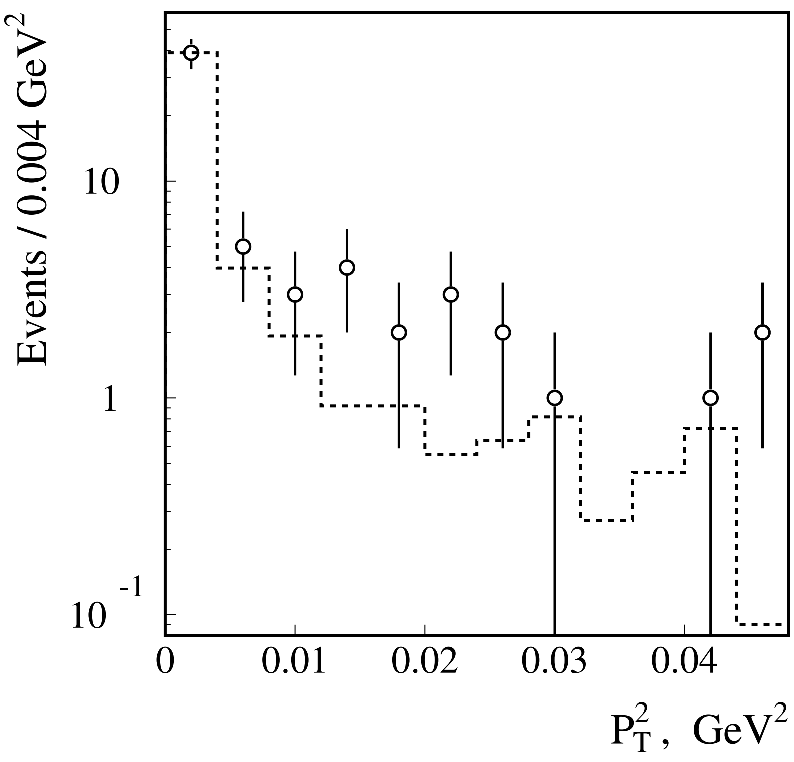

Figure 3: The P_T^2 distribution for events in the range $1370 < M(\mathrm{K^0_S}\,\mathrm{K}^{\pm}\pi^{\mp}) < 1560$ MeV. The GaGaRes Monte Carlo prediction (dashed histogram) is normalised to the number of data events (circles) in the first bin.

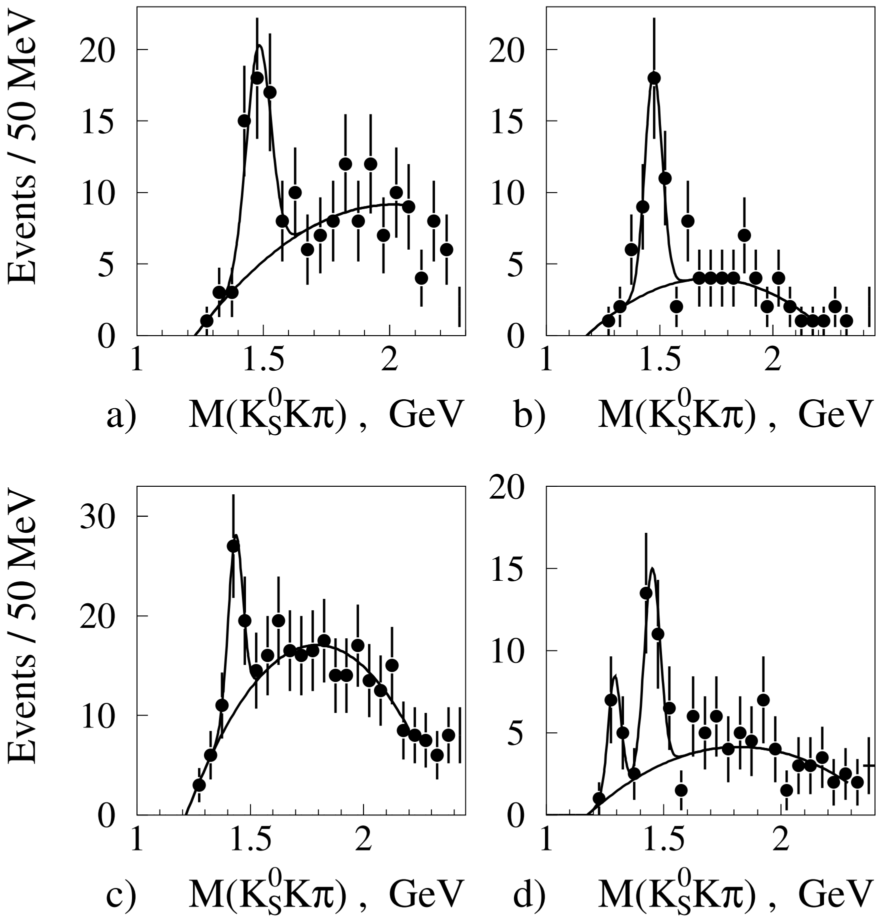

Figure 4: $K^0_S K^{\pm}\pi^{\mp}$ spectra for different P_T^2 bins. The two upper plots, a) $P_T^2 < 0.02$ GeV^2 and b) $0.02 < P_T^2 < 0.2$ GeV^2, are from the low P_T^2 selection sample. The two lower plots, c) $0.2 < P_T^2 < 1.$ GeV^2 and d) $1. < P_T^2 < 7.$ GeV^2, are from the high P_T^2 selection sample. The fits of a Gaussian peak plus polynomial background are superimposed to the data. In the highest P_T^2 bin, (d), also the peak of the $f_1(1285)$ is present and the fit contains two Gaussians.

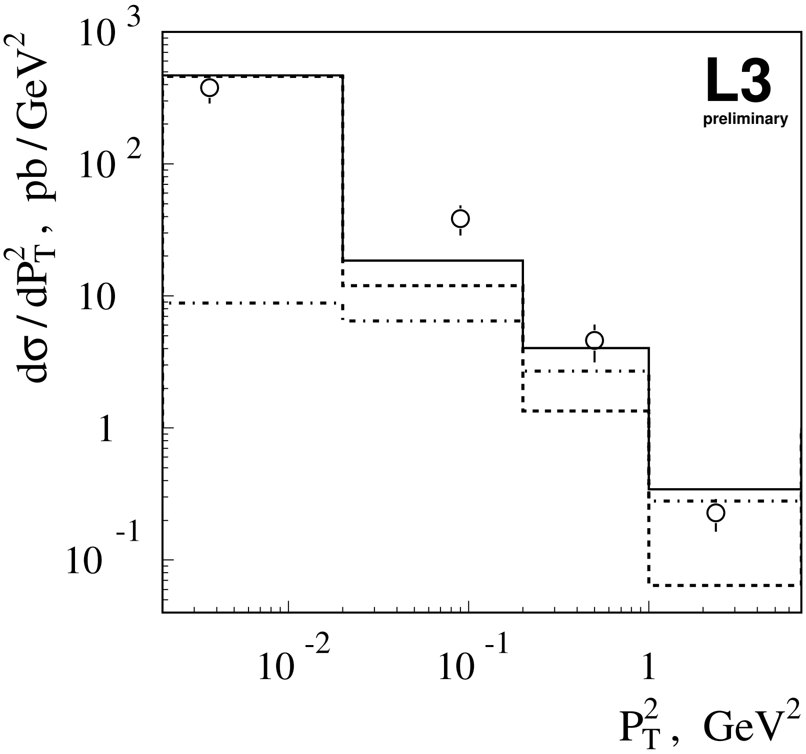

Figure 5: Differential cross section of the resonance signal at the mass around 1470 MeV observed in the previous figure.

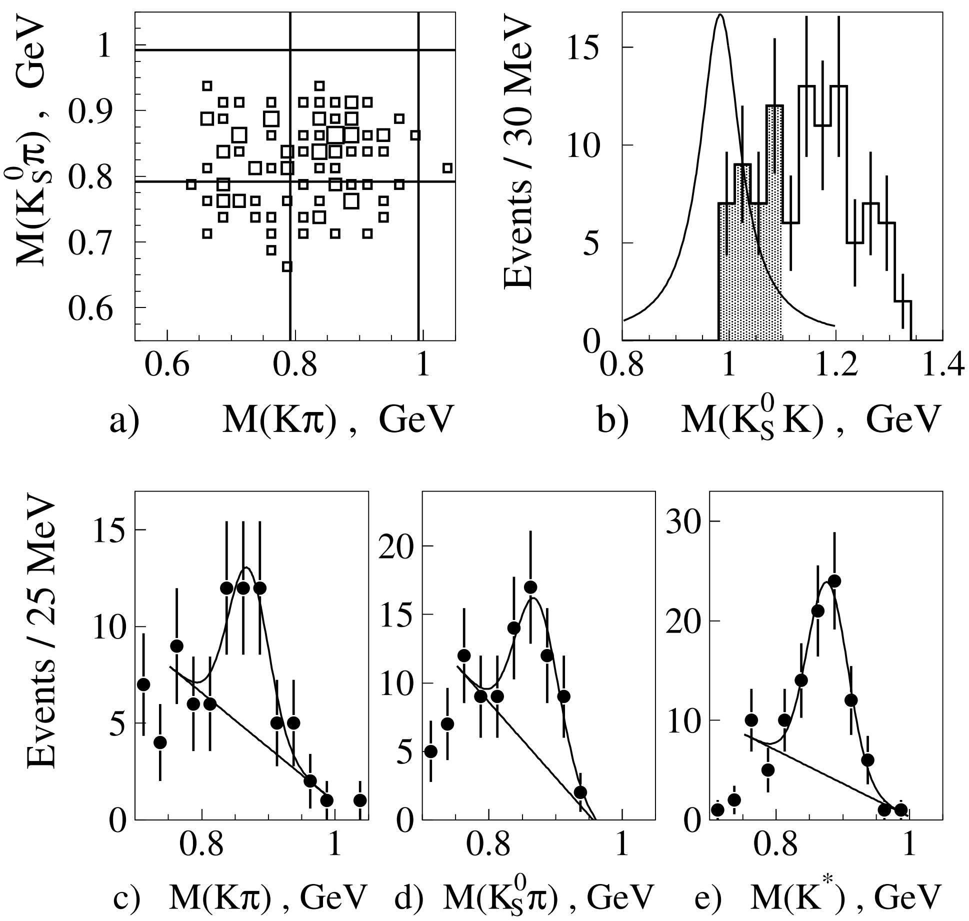

Figure 6: Search for the $K^*(892)\bar{K}$ and $a_0(980)\pi$ states in the $K^0_S K^{\pm}\pi^{\mp}$ sample for $P_T^2 < 0.2$ GeV^2 in the $\eta\,(1440)$ region ($1370 < M < 1560$ MeV). a) The scatter plot of masses of Kπ combinations with the $K^*(892)$ regions marked. b) The K^0_SK mass spectrum. A Breit–Wigner function with the $a_0(980)$ parameters is drawn with an arbitrary height. c) and d) The Kπ projections fitted with a Gaussian over a linear background. e) The Kπ combination with the mass closest to $K^*(892)$ fitted with a Gaussian over a linear background.

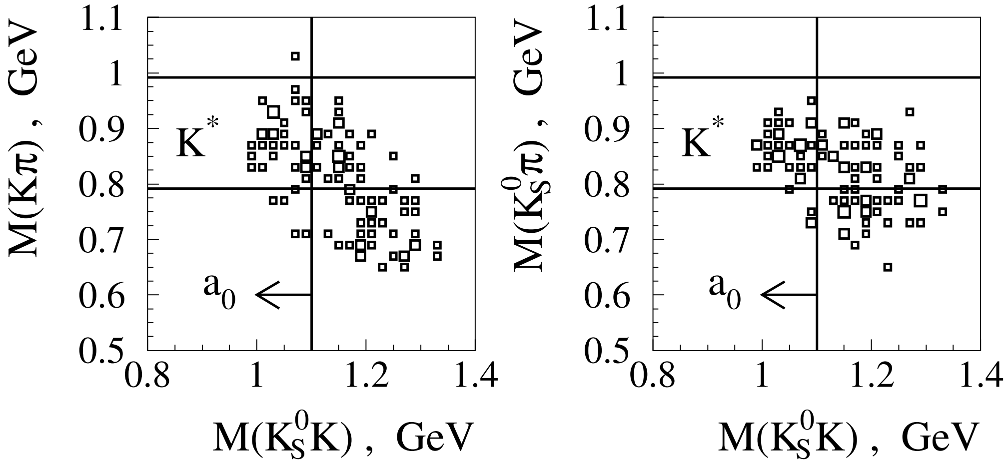

Figure 7: The scatter plots of $K^{\pm}\pi$ and $K^0_S\pi$ versus $K^0_S K$ masses for $P_T^2 < 0.2$ GeV^2 and $1370 < M(K^0_S\, K^{\pm}\pi^{\mp}) < 1560$ MeV.

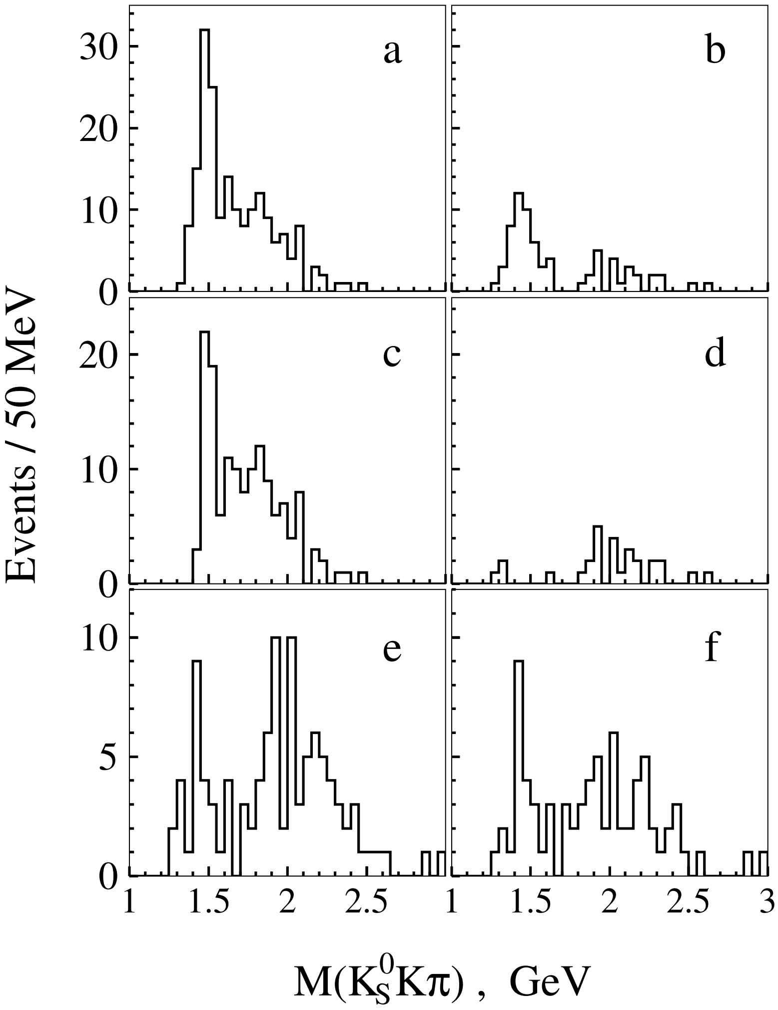

Figure 8: The $K_S^0 K^{\pm}\pi^{\mp}$ spectra at $P_T^2 < 0.2$ GeV^2:
a) For events when at least one $K\pi$–combination has mass ($792 < M(K\pi) < 992$ MeV) (K^*).
b) For events with $M(K_S^0 K) < 1100$ MeV (a_0). c) K^* no a_0. d) a_0 no K^*. e) No K^*. f) No K^* no a_0.

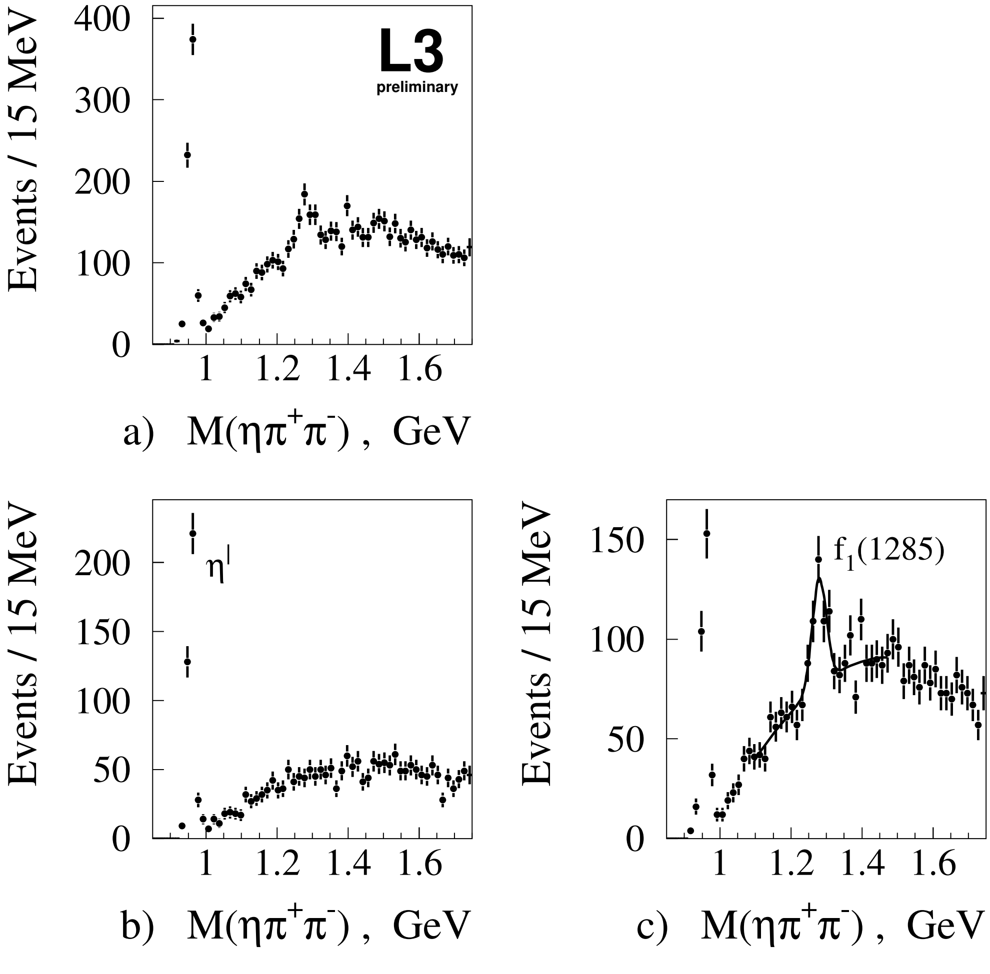

Figure 9: The $\eta\pi^+\pi^-$ mass spectra: a) total spectrum, b) $P_T^2 < 0.02$ GeV^2 and c) $P_T^2 > 0.02$ GeV^2.